Journal of Catalysis 343 (2016) 185–195

Contents lists available at ScienceDirect

Journal of Catalysis

journal homepage: www.elsevier.com/locate/jcat

Kinetic modeling and transient DRIFTS–MS studies of CO_2 methanation over Ru/Al_2O_3 catalysts

Xiang Wang, Yongchun Hong, Hui Shi, János Szanyi *

Institute for Integrated Catalysis, Pacific Northwest National Laboratory, Richland, WA 99352, USA

ARTICLE INFO

Article history:
Received 7 October 2015
Revised 16 January 2016
Accepted 1 February 2016
Available online 22 February 2016

Keywords:
CO_2 reduction
Ru/Al_2O_3
Particle size
Langmuir–Hinshelwood mechanism
Kinetic modeling

ABSTRACT

CO_2 methanation was investigated on 5% and 0.5% Ru/Al_2O_3 catalysts (Ru dispersions: ~18% and ~40%, respectively) by steady-state kinetic measurements and transient DRIFTS–MS. Methanation rates were higher over 5% Ru/Al_2O_3 than over 0.5% Ru/Al_2O_3. The measured activation energies, however, were lower on 0.5% Ru/Al_2O_3 than on 5% Ru/Al_2O_3. Transient DRIFTS–MS results demonstrated that direct CO_2 dissociation was negligible over Ru. CO_2 has to first react with surface hydroxyls on Al_2O_3 to form bicarbonates, which, in turn, react with adsorbed H on Ru to produce adsorbed formate species. Formates, most likely at the metal/oxide interface, can react rapidly with adsorbed H forming adsorbed CO, only a portion of which is reactive toward adsorbed H, ultimately leading to CH_4 formation. The unreactive CO molecules are in geminal form adsorbed on low-coordinated sites. The measured kinetics are fully consistent with a Langmuir–Hinshelwood type mechanism in which the H-assisted dissociation of the reactive CO^* is the rate-determining step (RDS). The similar empirical rate expressions ($r_{CH_4} = kP_{CO_2}^{0.1} P_{H_2}^{0.3-0.5}$) and DRIFTS–MS results on the two catalysts under both transient and steady-state conditions suggest that the mechanism for CO_2 methanation does not change with Ru particle size under the studied experimental conditions. Kinetic modeling results further indicate that the intrinsic activation barrier for the RDS is slightly lower on 0.5% Ru/Al_2O_3 than on 5% Ru/Al_2O_3. Due to the presence of unreactive adsorbed CO on low-coordinated Ru sites under reaction conditions, the larger fraction of such surface sites on 0.5% Ru/Al_2O_3 than on 5% Ru/Al_2O_3 is regarded as the main reason for the lower rates for CO_2 methanation on 0.5% Ru/Al_2O_3.

Published by Elsevier Inc.

1. Introduction

The utilization of C1 sources for the synthesis of hydrocarbons is of great significance with respect to environmental protection and development of renewable energy. Although there has been a tremendous amount of research in catalytic hydrogenation, most of this interest has been focused on the hydrogenation of CO over various transition metal catalysts [1]. The hydrogenation of CO_2, an abundant, renewable, yet relatively under-used C1 source, over these catalysts is at least of equal importance as a reaction relevant to the production of energy carriers [2,3]. The hydrogenation of CO_2 to methane without any net CO_2 emission not only provides a sustainable route for synthesizing useful chemicals and fuels, but also contributes to alleviating global climate changes induced by CO_2 emissions [4]. However, there have been considerably fewer systematic investigations on CO_2 methanation, compared with CO methanation. The CO_2 methanation reaction is an 8-electron process in which the fully oxidized carbon is reduced to its fully reduced form in methane, and there are significant kinetic barriers that require a catalyst to overcome in order to achieve acceptable rates and selectivities. Supported transition metal catalysts including Ni [5–10], Pd [11–15], Pt and Ir [12], Ru [12,16–28], and Rh [12,29–34] have been demonstrated to be active toward CO_2 methanation. However, key aspects regarding the mechanism of CO_2 methanation still remain elusive. For instance, CO_2 dissociation has been suggested as the rate-determining step (RDS) [31], while the more common belief is that the dissociation of adsorbed CO or hydrogenation of adsorbed CO is the RDS [17,25,35,36]. Furthermore, the reaction mechanism has been demonstrated to be strongly dependent on the identity of the metal, the nature of the support and reaction conditions.

Al_2O_3-supported Ru particles with a larger average size were found to be more active than those of a smaller average size for CO_2 methanation, as reported in our previous study [20]. The underlying principles governing this size dependence in Ru-catalyzed CO_2 methanation, however, were not fully understood at that time. In spite of the considerable efforts devoted to

* Corresponding author.
E-mail address: janos.szanyi@pnnl.gov (J. Szanyi).

http://dx.doi.org/10.1016/j.jcat.2016.02.001
0021-9517/Published by Elsevier Inc.

understanding the site requirement and elementary steps of CO_2 methanation over supported Ru catalysts, the detailed reaction mechanism, primarily the reaction pathway, the nature of key intermediates, the RDS and the mechanistic origin of the size effect of Ru, are still under debate. Solymosi et al. proposed that the methanation of CO_2 on 5 wt% Ru/Al_2O_3 occurs via the formation of surface carbon and its subsequent hydrogenation, and excluded the possibility of the dissociation of CO_2 as the RDS [17]. Furthermore, they pointed out that formate located on Al_2O_3 support was a spectator species in the methanation of CO_2. In contrast, Prairie et al. reported that formate species played a major role in the activation of CO_2 forming adsorbed CO via reverse water-gas shift reaction, and that the hydrogenation of adsorbed CO is rate-controlling during CO_2 methanation on both Al_2O_3 and TiO_2 supported Ru catalysts [28]. Similarly, Renken et al. also proposed a sequential conversion of surface species on Ru/TiO_2 from carbonate to formate then to adsorbed CO, which is subsequently hydrogenated to methane [26].

In-situ transient FTIR spectroscopy has been employed as a tool to uncover the mechanistic roles of the spectroscopically observable species in a number of studies, including the above literature precedents on supported Ru catalysts. However, the kinetic responses of surface species under transient conditions can be characteristically distinct from those obtained during steady-state reactions. On the other hand, steady-state rate measurements cannot yield direct information about the nature and coverage of surface intermediates. Therefore, it would be desirable to bring all these (transient and steady-state, *in situ* spectroscopic and reaction kinetic) approaches together in one integrated investigation to arrive at a more definitive picture of the studied catalytic reaction.

Herein, Ru/Al_2O_3 catalysts with low to medium Ru dispersions (18% and 40%) were employed in this study to avoid sintering of Ru particles during reaction, as small Ru clusters supported on Al_2O_3 can easily sinter during CO_2 methanation [20]. Combining kinetic measurements, performed over a wide range of reactant concentrations and temperatures, with analyses of transient *in situ* diffuse reflectance infrared Fourier transform spectroscopic (DRIFTS) and mass spectrometric (MS) experiments, a number of mechanistic sequences consistent with experimental observations were proposed. Kinetic modeling based on Langmuir–Hinshelwood type formalisms was applied to provide a quantitative description for the steady-state behavior, and, ultimately, to provide insights into the mechanism of CO_2 methanation on Ru/Al_2O_3.

2. Experimental

0.5 and 5 wt% Ru/Al_2O_3 catalysts were prepared with a commercial γ-Al_2O_3 powder (Sasol, Puralox SBA-200, BET specific surface area = 200 m^2/g) by the incipient wetness method using ruthenium (III) nitrosyl nitrate solution ($Ru(NO)(NO_3)_x(OH)_{3-x}$ in dilute nitric acid, 1.5% Ru, Aldrich) as the Ru precursor. After impregnation, the samples were dried in static air at 373 K for 24 h and stored under ambient conditions. The catalyst samples were activated prior to catalytic measurements by calcination at 773 K for 2 h in 6.7% O_2/He (flow rate = 60 mL/min) followed by reduction at 773 K for 1 h in 2% H_2/Ar (flow rate = 60 mL/min).

The number of exposed Ru surface atoms was determined from the volumetric uptake of CO at 313 K, using a Micromeritics AutoChem 2920 Chemisorption Analyzer. The catalysts were pretreated under identical condition to that applied prior to the catalytic tests. Because of the dominance of bridging CO* evidenced in IR spectra of CO adsorption on both samples, the $Ru_{surface}$:CO stoichiometry ratio of 2:1 was used for the estimation of Ru dispersions.

The catalytic reactions were carried out in a quartz packed-bed tubular reactor (1/4″ in o.d. and 5/32″ in i.d.) with plug flow hydrodynamics. The catalysts were pressed, crushed and sieved to 180–450 μm; typically, 15–60 mg of catalyst was diluted by SiC (180–450 μm) to ensure better heat transfer and sufficient bed lengths which minimize channeling effects. Kinetic measurements were conducted in the temperature range of 513–573 K, at a total pressure of 101 kPa and gas hourly space velocities (GHSVs) of 33,000–135,000 mL g^{-1} h^{-1}. The gas mixture fed into the reactor contained 10–70% CO_2 and 70–10% H_2 in He balance, at a total flow rate of 60 mL/min. All gases were of ultrahigh purity and were further purified by passing them through oxygen and moisture traps (Supelpure®-O Oxygen/Moisture Trap, Sigma-Aldrich) installed on the feed lines. The CO_2 conversion was kept at <5.5%. No conversion of reactants was detected in blank runs with γ-Al_2O_3 under the testing conditions applied. The absence of thermal and diffusional gradients in catalyst bed was confirmed by the method suggested by Koros and Nowak [37]. Thermodynamic calculation results also suggested that reactions were operated far from equilibrium limitation under testing conditions. The reactor effluent was analyzed with an on-line Agilent HP 7820 gas chromatograph equipped with a capillary column (Supelco, Carboxen 1010 PLOT, 30 m × 0.53 mm i.d.) and a thermal conductivity detector.

In situ FTIR spectra were collected on a Mattson Research Series 1000 FT-IR spectrometer equipped with a DRIFTS accessory and a high temperature cell (Harrick). Each spectrum was recorded at 4 cm^{-1} resolution, averaged over 64 scans, and reported as pseudo-absorbance [38]. The Ru/Al_2O_3 powders were placed into the sample holder cup of the high temperature cell without packing or dilution. Prior to spectral acquisition at 503 K, the catalyst sample was reduced in H_2 at 673 K for 1 h and then cooled down in He flow and kept being purged by He at room temperature for 2 h. Then a background IR spectrum was recorded at 503 K reaction temperature in He with a flow rate of 20 mL/min. A gas feeding manifold, equipped with electronic mass flow controllers (Brooks), was used to introduce gases with controlled flow rates and compositions. For the transient experiments, gases (He, 2% CO_2/He, 8% H_2/He and their mixture) with a flow rate of 20 mL/min were introduced to the cell and switched when needed. DRIFT spectra were recorded every ~90 s. The effluent gas of the cell was analyzed by a mass spectrometer monitoring m/z = 44 (CO_2), 2 (H_2), 15 (CH_4), 18 (H_2O) and 28 (CO) with a response time of less than 1 s.

The interaction of CO_2 with 5% Ru/Al_2O_3 sample was evaluated by FTIR measurements with a Bruker Vertex 80 spectrometer equipped with a static, batch-type sample cell and a liquid nitrogen-cooled MCT detector operated in transmission mode. Each spectrum was recorded at 4 cm^{-1} resolution, and was averaged over 256 scans. The sample cell is a 2¾″ stainless steel cube equipped with KBr windows and connected to pumping stations and a gas handling system. The sample holder rod has a ceramic feedthrough for heating and thermocouple connections. The powder Ru/Al_2O_3 samples were pressed onto a tungsten mesh (>80% light transmission) which was attached to copper heating legs allowing resistive heating of the samples. The pressure in the IR cell can be controlled between 2.6×10^{-9} and 101 kPa. CO_2 was purified by cycles of freeze/pump/thaw prior to adsorption measurements. In a typical procedure, the sample was first pre-treated in H_2 and then in vacuum, both at 773 K, and then cooled to the desired temperature where the adsorption experiments were carried out. CO_2 was added to the cell in a stepwise manner and a FTIR spectrum was collected upon equilibration after each CO_2 aliquot.

Regression of experimental data was performed using Microsoft EXCEL Solver with GRG nonlinear engine for nonlinear functions. For data obtained at each temperature, a set of parameters (rate and equilibrium constants) was fitted with the least squares as target function. The temperature dependences of rate and

equilibrium constants obtained were fitted by linear regression for the calculation of energetic parameters (enthalpies).

3. Results and discussion

3.1. Reaction kinetics

The dispersions of Ru estimated from CO chemisorption were ~40% and ~18% for the 0.5 and 5 wt.% Ru/Al_2O_3 catalysts, respectively. Kinetic measurements were conducted in the temperature range of 513–573 K and in a wide range of partial pressures of H_2 and CO_2 (10–70 kPa). The only products on both catalysts are CO, CH_4 and H_2O under testing conditions. Fig. 1a shows the turnover frequencies (TOFs) for CH_4 formation (i.e., the formation rates of CH_4 normalized to the number of surface Ru atoms), plotted against the inverse temperature at a molar ratio of $H_2/CO_2 = 4$ (the stoichiometric H_2/CO_2 ratio for CO_2 methanation) on 0.5% and 5% Ru/Al_2O_3. Larger Ru particles appeared to be more catalytically active than smaller particles for CH_4 formation under testing conditions, consistent with our previous observations [20]. For instance, the TOFs for CH_4 formation at 553 K were 0.043 and 0.068 s^{-1} on the 0.5% and 5% Ru/Al_2O_3 catalysts, respectively.

Solymosi et al. reported a TOF of 0.194 s^{-1} for CO_2 methanation, on a 5% Ru/Al_2O_3 catalyst (D_{Ru} = ~5%) at $H_2/CO_2 = 4$ and 548 K [17]. This value is higher than ours (0.068 s^{-1} at 553 K) on the 5% Ru/Al_2O_3 catalyst of a higher dispersion (D_{Ru} = 18%), showing a trend that a lower rate is expected on smaller particles. The selectivity to methane was reported to be >98% in the temperature range of 443–503 K [17]. Under all conditions studied in this work, the selectivity to methane was always >90% on both Ru/Al_2O_3 catalysts. For instance, the selectivity to methane was ~96% on 5% Ru/Al_2O_3 and 93% on 0.5% Ru/Al_2O_3 at $H_2/CO_2 = 4$ and 553 K, which is in good agreement with the previous work [17]. The CO formation rates are negligible compared with the formation rate of CH_4 at all testing conditions. Therefore, the CO formation side reaction and its potential impact on the kinetics were ignored in the further discussion of methanation kinetics.

The apparent activation energies determined under a wide range of partial pressures of H_2 and CO_2 are shown in Fig. 1b. For 5% Ru/Al_2O_3 (D_{Ru} = 18%), the apparent activation energy (64–80 kJ/mol) for CH_4 formation decreased with decreasing H_2 pressure (at a fixed CO_2 pressure), but stayed essentially constant with changing CO_2 pressure (at a fixed H_2 pressure). In addition, the apparent activation energy (57–70 kJ/mol) for CH_4 formation over 0.5% Ru/Al_2O_3 (D_{Ru} = 40%) was lower than that on 5% Ru/Al_2O_3. Similarly, Weatherbee and Bartholomew reported an apparent activation energy of 72 kJ/mol for CO_2 methanation on 0.5% Ru/SiO_2 (D_{Ru} = 47%) between 502 and 563 K at atmospheric pressure (H_2/CO = 4:1) [25]. In another work, an apparent activation energy of 71 kJ/mol was reported on a 0.5% Ru/Al_2O_3 catalyst under similar conditions [19].

Table 1 shows the dependences of CH_4 formation rate on CO_2 and H_2 partial pressures for both catalysts. The apparent reaction order with respect to CO_2 was 0.12 ± 0.05 for both catalysts, almost independent of reaction temperature and Ru dispersion. However, it showed a monotonic increase with increasing H_2 pressure. The H_2 pressure dependence of apparent reaction order with respect to CO_2 can be explained by competitive adsorption between H_2 and CO_2: a higher H_2 pressure results in a higher coverage of adsorbed H atoms (H^*) and lower coverages of CO_2-derived intermediates, leading to a higher reaction order with respect to CO_2.

The apparent reaction order with respect to H_2 varied from ~0.3 to ~0.5 on both catalysts. Similarly, a monotonic increase with increasing CO_2 pressure was observed. However, the effect of temperature on the H_2 reaction order is more pronounced than that on the CO_2 reaction order. The apparent reaction order with respect to H_2 increases monotonically with increasing temperature. This can be explained with a decreasing coverage of adsorbed H atoms (H^*) at elevated temperature due to the exothermic nature of dissociative H_2 chemisorption. An empirical rate equation for CH_4 formation based on the power rate law can be thus generalized as $r_{CH_4} = kP_{CO_2}^{0.1} P_{H_2}^{0.3-0.5}$ for both catalysts at all reaction conditions studied.

3.2. In situ transient DRIFTS–MS measurements

In order to identify key surface species that are mechanistically relevant to CO_2 methanation, a series of DRIFTS–MS measurements were carried out under transient conditions by switching between different gas streams (He, H_2, CO_2 or $CO_2 + H_2$) at 503 K.

Fig. 2 shows a series of *in situ* FTIR spectra recorded during CO_2 exposure (Fig. 2a), subsequent purge with He (Fig. 2b) and finally with H_2 (Fig. 2c) of a 5% Ru/Al_2O_3 catalyst sample. The effluent gas composition during this series of experiments monitored by MS is presented as a function of time-on-stream in Fig. 2d. The IR features developing during CO_2 exposure (Fig. 2a) are related

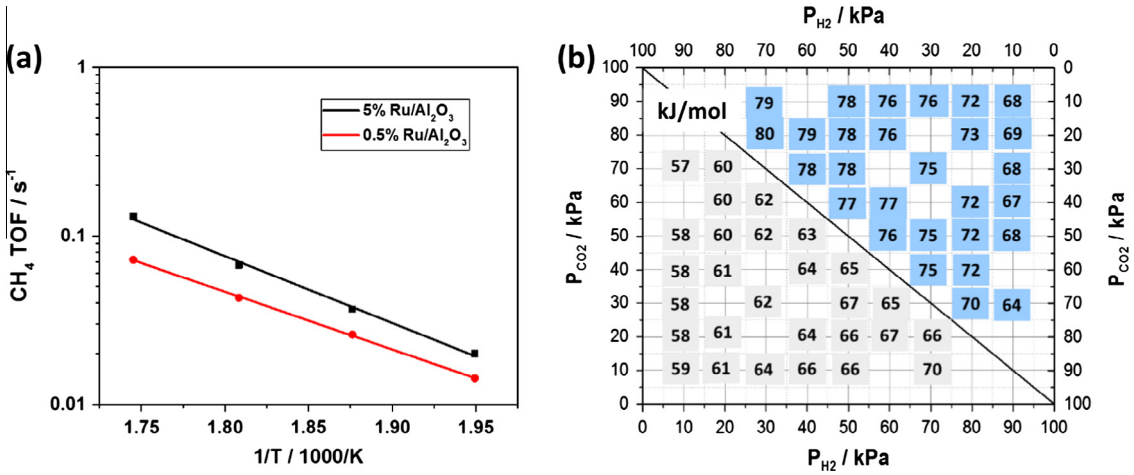

Fig. 1. Turnover frequencies (TOFs) of (a) CH_4 formation as a function of reciprocal temperature at 513–573 K on 5% and 0.5% Ru/Al_2O_3 in a flow containing 40% H_2 and 10% CO_2 in He balance (101 kPa total) at a total flow rate of 60 mL/min. (b) Apparent activation energies for CH_4 formation in CO_2 hydrogenation over 5% Ru/Al_2O_3 (blue in right-up) and 0.5% Ru/Al_2O_3 (gray in left-down) under different partial pressures of H_2 and CO_2 at a total flow rate of 60 mL/min.

Table 1
The reaction orders for CH_4 formation rate with respect to CO_2 and H_2 pressures during CO_2 methanation on 5% and 0.5% Ru/Al_2O_3 at 513–573 K and different partial pressures of CO_2 and H_2 (10–50 kPa for both, total pressure 101 kPa balanced with He).

Catalyst	T/K	Order in CO_2 with constant P_{H2}/kPa					Order in H_2 with constant P_{CO2}/kPa				
		10	20	30	40	50	10	20	30	40	50
5% Ru/Al_2O_3	**513**	0.14	0.15	0.17	0.16	0.20	0.33	0.36	0.39	0.39	0.40
	533	0.12	0.14	0.17	0.18	0.18	0.37	0.40	0.43	0.44	0.47
	553	0.12	0.16	0.17	0.18	0.19	0.42	0.45	0.48	0.50	0.52
	573	0.11	0.13	0.16	0.17	0.19	0.47	0.50	0.53	0.56	0.55
0.5% Ru/Al_2O_3	**513**	0.07	0.11	0.13	0.15	0.16	0.27	0.31	0.35	0.37	0.39
	533	0.07	0.09	0.12	0.15	0.15	0.30	0.34	0.38	0.41	0.45
	553	0.03	0.09	0.10	0.12	0.14	0.34	0.39	0.43	0.45	0.48
	573	0.06	0.08	0.10	0.12	0.15	0.41	0.42	0.46	0.48	0.50

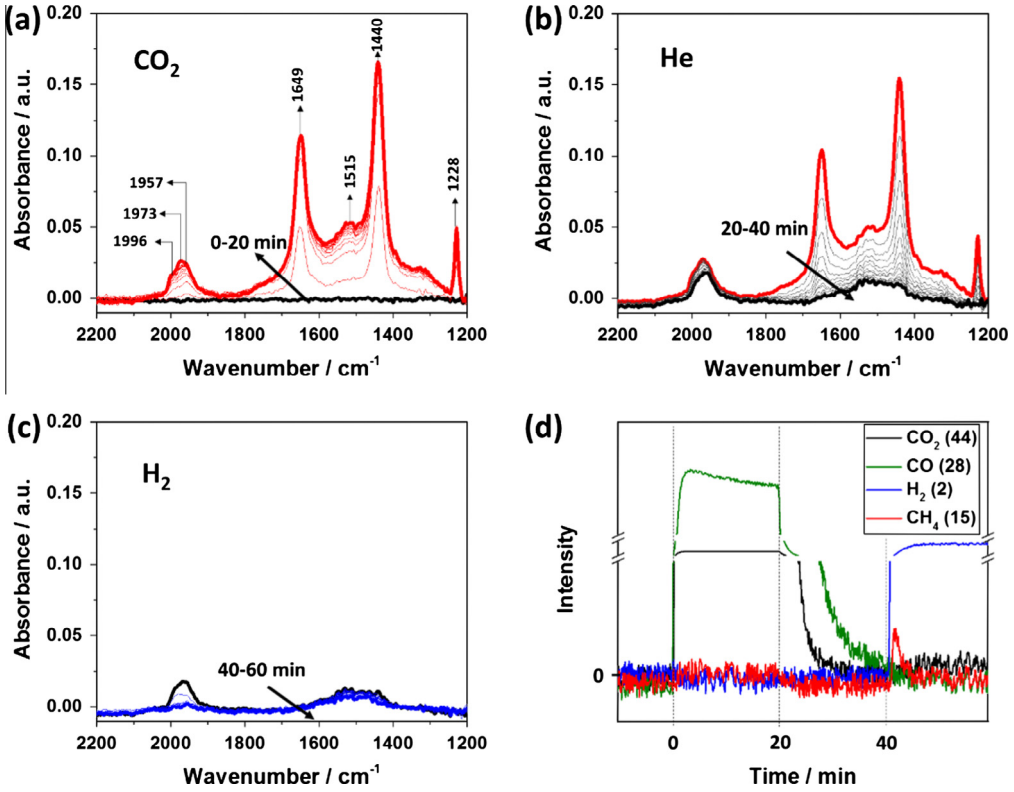

Fig. 2. DRIFT spectra collected at 503 K when the feed gas was switched (a) from He to CO_2 followed by a switch back to (b) He and then to (c) H_2 over 5% Ru/Al_2O_3. (d) The corresponding MS signals obtained at the exit of the DRIFT cell as a function of time.

to adsorbed species on alumina support and the Ru particles, as well as to gas phase CO_2 (2349 cm^{-1}, data not shown). The IR bands at 1228, 1440 and 1649 cm^{-1} represent different vibrational modes of alumina-adsorbed bicarbonates [39–42], and the 1515 cm^{-1} band is characteristic of carbonates [41–45]. It was reported that bicarbonates and carbonates are generated from the reaction between CO_2 and hydroxyl group on the Al_2O_3 support [46,47]. IR absorption bands appearing at 1996, 1973 and 1957 cm^{-1} upon CO_2 exposure are assigned to adsorbed CO on Ru in multi-bound forms (bridging and three-folded). Although the Ru/Al_2O_3 sample was purged with flowing He for 2 h after being reduced in H_2, formation of adsorbed CO on Ru surface via reaction between CO_2 and residual H^* may not be totally avoided, as reported in our previous work of CO_2 reduction on Pd/Al_2O_3 [15]. In order to address the possible role of residual adsorbed hydrogen on the formation of CO^* on Ru, the interaction of CO_2 with the 5% Ru/Al_2O_3 sample was studied by transmission FTIR in a static cell. The absence of adsorbed H on the surface of Ru particles before introducing controlled amounts of CO_2 was guaranteed by evacuating the cell to 2.6×10^{-9} kPa for 2 h after H_2-reduction at 773 K. Fig. S1 clearly shows that only trace amount of adsorbed CO was formed on Ru/Al_2O_3 without adsorbed H on the surface, while a large amount of adsorbed CO was produced from CO_2 in the presence of adsorbed H on the surface of Ru particles. Therefore, we do not exclude the possibility that adsorbed CO could be formed by direct dissociation of CO_2 on Ru (possibly on low-coordination sites), but it is clear that the H-assisted CO_2 dissociation is much more facile and is the dominant pathway for adsorbed CO formation during CO_2 methanation on Ru/Al_2O_3. It was also shown in a recent theoretical study that on Ru(0001) surface, the direct dissociation of CO_2 is thermodynamically favorable (−0.92 eV) but with a significant activation barrier (1.20 eV) [23], suggesting the direct CO_2 dissociation does not readily occur on close-packed Ru surfaces that are abundant in large Ru particles. During the CO_2 flow period (0–20 min), neither CH_4 nor CO was detected by MS (Fig. 2d). Note that the 28 amu MS signal in the 0–40 min of

time-on-stream completely accounts for the contribution of CO_2 from its fragmentation in the ionizer of the mass spectrometer, as no CO formation was detected by GC in the plug-flow reactor under the same conditions.

Fig. 2b shows a rapid decrease and disappearance of all the IR features representing adsorbed bicarbonates and carbonates in He purge at 503 K. This is similar to that observed previously on Pd/Al_2O_3 [15]. The adsorbed bicarbonates on the Al_2O_3 support are unstable and decompose to gaseous CO_2 in He purge at this temperature. In contrast, the intensities of adsorbed CO bands only slightly decreased even after 20 min purging with He. Therefore, we conclude that dissociation of CO^* hardly occurs in He; instead, the small decrease of CO^* features in IR spectra should be mainly attributed to desorption of a small fraction of CO^* in He purge at 503 K. CH_4 formation was also not detected by MS in this period, as shown in Fig. 2d (t = 20–40 min).

The H_2 flow was introduced into the IR cell when there was no further decrease in IR absorption band intensities of the features associated with carbonates, and the corresponding spectra (40–60 min) are shown in Fig. 2c. A much faster decrease and subsequent disappearance of the IR absorption band intensity for adsorbed CO species (1850–2100 cm^{-1}) were observed upon exposure to H_2 compared with the intensity decay of this band in He in Fig. 2b, while the intensities of carbonate-related absorption bands remained almost unchanged. Concomitant with the disappearance of the IR signature of adsorbed CO is the appearance of a sharp peak of CH_4 (15 amu) in the mass spectrum of the effluent gas stream (Fig. 2d; t = 40 min). Furthermore, the formation of CH_4 ceased as soon as the IR signals of adsorbed CO disappeared, clearly indicating that the adsorbed CO is converted only in the presence of H_2, and CH_4 is produced as a result of the hydrogenation of CO^* species. A similar phenomenon was observed by Marwood et al., i.e., adsorbed CO on Ru/TiO_2 catalyst was reactive in H_2 and was claimed to be an intermediate for CH_4 formation [26]. Likewise, adsorbed CO was also demonstrated to be an intermediate to CH_4 formation in our previous study on CO_2 methanation over Pd/Al_2O_3 [15].

In order to investigate the transformation of surface species generated under steady state reactions in H_2 or CO_2, transient experiments in which the feed gas was switched from a reactant gas mixture ($CO_2 + H_2$) to the individual reactant of H_2 or CO_2 were performed. Fig. 3a shows the evolution of IR bands for surface species on the 5% Ru/Al_2O_3 sample at 503 K upon switching from $CO_2 + H_2$ to CO_2 stream. Under the flow of $CO_2 + H_2$ (0 min, steady state, black trace in Fig. 3a) at 503 K, intense IR features developed at 1375, 1392 and 1593 cm^{-1} (not present in Fig. 2a), which are characteristic of adsorbed formate species [35]. Moreover, the intensity of bicarbonate features (1649, 1440 and 1228 cm^{-1}) became weaker compared with those observed in CO_2 flow in Fig. 2a. In our previous study of CO_2 methanation on Pd/Al_2O_3, bicarbonates were found to be intermediates to the formates via the reaction with adsorbed H on Pd particles. Our results here suggest that the same mechanism for the conversion of bicarbonates to formates holds for Ru/Al_2O_3 as well. The IR (cf. Figs. 2 and 3) results have shown that only bicarbonate can be formed in the presence of CO_2 without H_2 (Fig. 2a), while formate and adsorbed CO were observed in $CO_2 + H_2$ (the black trace in Fig. 3a). Given the above discussion that CO(ads) leads to CH_4 product rather than formate species on the support (Fig. 2c and d), it is clearly demonstrated that the dominant pathway for the formate formation is the reduction of bicarbonate with H^*. Here, it is pertinent to mention the result of a theoretical study showing that adsorbed CO_2 on the Ru(0001) surface prefers to first undergo hydrogenation to formate (E_a = 0.41 eV), rather than dissociation via carboxylic intermediate (E_a = 1.04 eV to trans-COOH and 1.12 eV to cis-COOH) [23].

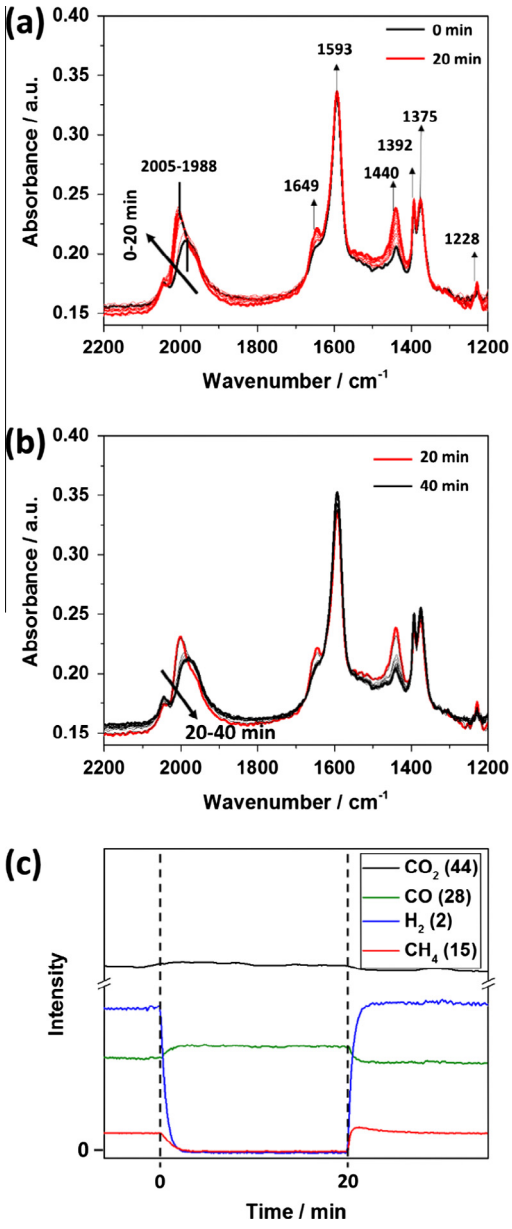

Fig. 3. DRIFT spectra collected at 503 K while the feed gas was switched (a) from $CO_2 + H_2$ (t = 0 min) to CO_2 followed by a switch back (b) from CO_2 (t = 20 min) to $CO_2 + H_2$ over 5% Ru/Al_2O_3. (c) The corresponding MS signals obtained at the exit of the DRIFT cell as a function of time.

Furthermore, it is worth noting that the intensity of adsorbed CO (1900–2010 cm^{-1}) in the $CO_2 + H_2$ flow (0 min, Fig. 3a) was higher by a factor of 2 than that in Fig. 2a where the sample was exposed to a CO_2 flow, apparently caused by the different concentrations of adsorbed H on Ru particles. During this period, the CH_4 concentration was constant in the effluent (Fig. 3c, red trace). The formation of CO as a gaseous product could not be verified, because the 28 amu signal from CO_2 fragmentation in the MS prevented us from unambiguously distinguishing CO produced by the reaction at low CO_2 conversions and low CO selectivities on Ru/Al_2O_3.

Following the switch from $CO_2 + H_2$ to CO_2 at t = 0 min, the band intensities of adsorbed bicarbonates and adsorbed CO increased rapidly to new steady levels with the decrease in the partial pressure of H_2, while the band intensities of formates did not change at all (red traces in Fig. 3a). However, after switching back to $CO_2 + H_2$ at 20 min (black traces in Fig. 3b), these band intensities of absorbed bicarbonate and adsorbed CO bands decreased to the

same levels as before in the steady-state reaction (black trace in Fig. 3a), while those of the formates still remained unaffected. Taking into account the main locations of bicarbonates and H* (Al_2O_3 support and the Ru metal, respectively), the decrease in intensity of bicarbonate bands in Fig. 3b was most possibly caused by the reaction between bicarbonates and adsorbed H occurring at the interface of Ru particles and the Al_2O_3 support.

As we have mentioned earlier, both the formation and consumption of adsorbed CO required the assistance of H*. Furthermore, the monotonic increase in IR band intensity of adsorbed CO with decreasing H_2 pressure points to the competitive adsorption between H* and CO*. With the removal of H_2 (Fig. 3a), more surface sites become available for adsorbed CO to form, whose surface concentration increases until there is no more H* available to affect the adsorbed CO* (both in terms of formation and consumption). Upon the re-introduction of H_2, the surface concentration of CO* decreased (Fig. 3b), as a result of the re-established equilibrium between available surface sites, gaseous H_2 and CO_2. Fig. 3c shows the evolution of the MS signals in effluents during alternate switches. CH_4 concentration decreased to zero as soon as H_2 was removed completely, and was immediately re-established to the steady-state level with the switch back to the $CO_2 + H_2$ reactant gas mixture at $t = 20$ min.

Fig. 4a shows the evolution of IR bands for surface species upon switching from $CO_2 + H_2$ gas mixture to H_2 under reaction conditions on the 5% Ru/Al_2O_3 sample. The intensities of IR bands representing adsorbed CO, formate and bicarbonate all decreased as the CO_2 flow was cut off. In particular, the bands attributed to bicarbonates completely disappeared after 5 min in H_2 flow. It is worth noting that the disappearance of bicarbonates is faster than that in He purging (Fig. 2b), indicating the bicarbonate may migrate toward and react with adsorbed H present on Ru particles. As suggested in our previous work in CO_2 reduction over Pd/Al_2O_3, the slight decrease in the IR intensity of formate bands is due to the reaction between formates located at the interface of Ru/Al_2O_3 and adsorbed H on the Ru. Both Solymosi et al. and Marwood et al. concluded that most of the formates are located on the support and originate from the migration of formates formed at the metal/oxide interface by the reaction of bicarbonates (on the support) and dissociated H_2 (on the metal) toward the support due to the concentration gradient [26,48]. The formate is reactive toward the formation of adsorbed CO when it is close to or on Ru particles. However, formate species far from the metallic Ru can react with adsorbed H only very slowly, as their migration to the metal/oxide interface is energetically demanding [26,48]. Non-uniform reactivities of surface formate species on supported Co catalysts have been shown by Meunier et al. by plotting the natural logarithm of the characteristic IR band intensities of formates as a function of time [49,50]. The decay of the IR signal intensity for formate surface species as a function of time exhibited two distinct regimes: after switching from a $CO + H_2$ mixture to H_2 they observed an initial fast decrease in the IR band intensities of formates followed by a slow decrease. They explained these two regimes by the presence of two types of formate species with vastly different reactivities. Following a similar data treatment described in Refs. [49,50], we plotted the logarithm of the formate band intensities between 1410 and 1338 cm^{-1} as a function of time after the $CO_2 + H_2$ gas mixture was switched to H_2 (Fig. S2). The two separate processes of formate decomposition further suggest that two types of formates were initially present: one was close to Ru particles, while the other one was distant from Ru particles.

The decrease in the IR intensities of adsorbed CO bands after switching from $CO_2 + H_2$ to H_2 is due to the consumption of CO* via hydrogenation to form CH_4 based on the conclusion from Fig. 2. More importantly, only the CO* species at 1978 cm^{-1} gradually disappeared over time (Fig. 4a). No more CH_4 was detected

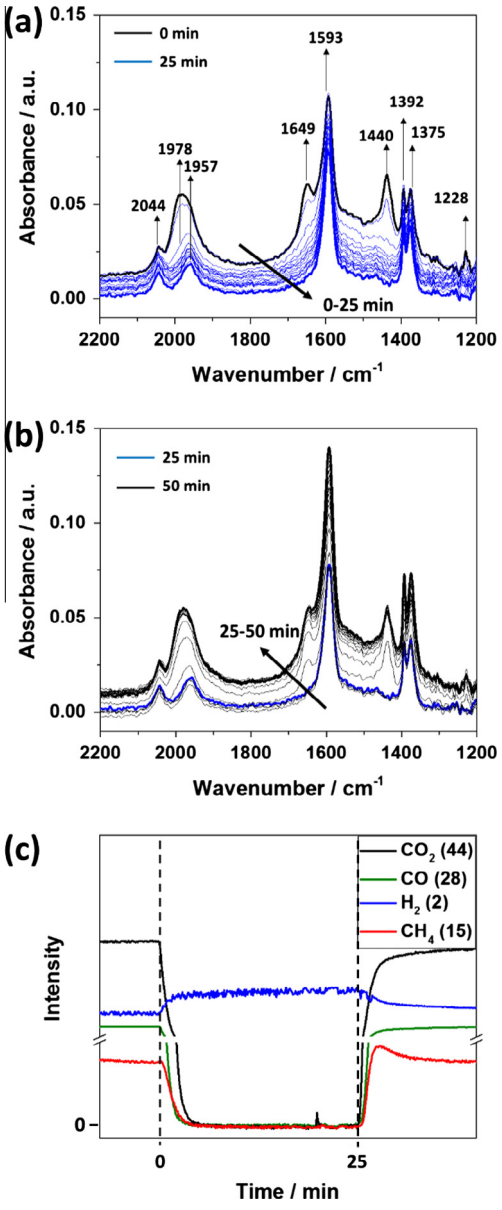

Fig. 4. DRIFT spectra collected at 503 K when the feed gas was switched (a) from $CO_2 + H_2$ ($t = 0$ min) to H_2 followed by a switch back (b) from H_2 ($t = 25$ min) to $CO_2 + H_2$ over 5% Ru/Al_2O_3. (c) The corresponding MS signals obtained at the exit of the DRIFT cell as a function of time.

in the effluent of the reactor after the disappearance of adsorbed CO at 1978 cm^{-1}. The adsorbed CO showing bands at 2044 and 1957 cm^{-1} did not disappear even after 25 min in H_2 flow. Similarly, Behm et al. found that when adsorbed CO on Ru/Al_2O_3 formed in CO methanation condition was exposed to flowing H_2/N_2, the broad band of adsorbed CO decreased but did not disappear completely [51]. Even after 1000 min of exposure to H_2/N_2, the two bands at 2040 and 1960 cm^{-1} were still present. They attributed the two bands to linear and bridging bonded CO*, respectively, but they were unable to explain their persistence to hydrogenation. These stable species were in some cases interpreted as adsorbed CO in disordered phase [26]. However, in view of results from prior literature on the two peaks at 2044 and 1967 cm^{-1} with the integrated intensity ratio of ~1 [52–54], we attribute these stable CO(ads) to be geminal di-carbonyls (i.e., $Ru(CO)_2$) adsorbed on low coordination Ru sites. Due to the coordinative saturation of these Ru sites, H_2 dissociation on these $Ru(CO)_2$ species is

suppressed, resulting in the high stability (inactivity toward further hydrogenation) of the CO* species. Therefore, these gem-dicarbonyls cannot be considered as reactive intermediates in CH_4 formation, as evidenced by the lack of correlation between their IR band intensities and CH_4 formation (MS).

As the feed was switched back to $CO_2 + H_2$, the intensities of all infrared bands representing reactive CO*, bicarbonates, as well as formates, gradually recovered (at 50 min; Fig. 4b) to the levels observed at $t = 0$ min. The CO* band at 1978 cm^{-1} increased rapidly and overlapped with the one at 1957 cm^{-1}, and combining into one broad band as it was in the spectrum at $t = 0$ min. CH_4 formation rate rapidly reached the same steady-state level as it was at $t = 0$ min (Fig. 4c). All these observations show that the changes in the coverages of key surface species are fully reversible during *in situ* DRIFTS experiments on 5% Ru/Al_2O_3.

The same set of surface species and qualitatively similar evolution patterns were observed during the series of transient *in situ* DRIFTS experiments on the 0.5% Ru/Al_2O_3 catalyst performed in the same way as for the 5% Ru/Al_2O_3 catalyst sample. The DRIFTS spectra recorded in these experiments are shown in Figs. S3–S5. However, during the steady-state reaction condition, some differences shown in Fig. 5a were noticed in the IR band position and intensity for adsorbed CO, possibly associated with the different average particle sizes of Ru in the two samples. For example, larger Ru particles on 5% Ru/Al_2O_3 have more terrace sites which favor the formation of bridging bonded CO*, whereas 0.5% Ru/Al_2O_3 has more highly dispersed Ru sites which favor the formation of geminal di-carbonyls. Another difference is observed in the 1200–1800 cm^{-1} region during the steady-state reaction, i.e., the IR band intensity of bicarbonates was higher, while that of formate species (after subtracting the contribution from the overlapping bicarbonate bands) was lower, on 0.5% Ru/Al_2O_3 than those on 5% Ru/Al_2O_3. Both species are associated with the Al_2O_3 support. Note that this phenomenon is analogous to that observed on 0.5% and 5% Pd/Al_2O_3 in our previous study: 0.5% Pd/Al_2O_3 catalyst provides fewer surface sites for H* to react with bicarbonates to form formate, which, in turn, gives rise to a lower band intensity of formate and a higher band intensity of bicarbonate in a IR spectrum [15]. The same explanation seems to be valid for the Ru/Al_2O_3 samples.

Fig. 5b shows the IR spectra collected after 20 min in H_2 following a switch from the steady-state reaction in $CO_2 + H_2$ on 5% and 0.5% Ru/Al_2O_3. While a fraction of CO* is rapidly converted in H_2 to CH_4 (Figs. 4 and S5), the geminal di-carbonyl present in Fig. 5b is stable and unreactive, as discussed above. As inferred from the integrated intensity (Fig. 5b), the concentration of these geminal di-carbonyl on 0.5% Ru/Al_2O_3 is much larger than that on 5% Ru/Al_2O_3. Moreover, from the transient DRIFTS experiment switching from $CO_2 + H_2$ to H_2 (Figs. 4a and S4a), the concentration of reactive CO* is lower on 0.5% Ru/Al_2O_3 than that on 5% Ru/Al_2O_3. The fraction of inactive surface Ru sites that do not contribute to catalytic turnovers for CO_2 methanation is larger on 0.5% Ru/Al_2O_3 than that on 5% Ru/Al_2O_3. This is one of the reasons for the lower "apparent" turnover rate (normalized on basis of all exposed surface atoms, rather than the "active" surface atoms) on 0.5% Ru/Al_2O_3 than on 5% Ru/Al_2O_3 during CO_2 hydrogenation, despite the slightly lower apparent activation energy over 0.5% Ru/Al_2O_3.

Overall, the similar evolution profiles of surface species observed during the transient FTIR spectroscopic experiments, and the similar reaction orders and activation energies during steady-state reactions on the two Ru/Al_2O_3 catalysts indicate that the mechanism of CO_2 methanation on both Ru/Al_2O_3 catalysts is identical, irrespective of their different average Ru particle sizes. Our results presented above have clearly demonstrated that the activation of CO_2 on Ru/Al_2O_3 catalysts did not occur measurably via direct dissociation to CO* and O*; rather, it proceeds through a bicarbonate intermediate, which, in turn, reacts with adsorbed hydrogen, as concluded for Pd/Al_2O_3. This reaction possibly occurs at the interface of Ru and Al_2O_3 and the product is most likely formate. Those formate species at the interfacial sites are reactive toward adsorbed H to form adsorbed CO. However, due to the slower rate of consumption than the rate of formation, the formate accumulates at the interface and migrates toward Al_2O_3 support due to its concentration gradient [26,48]. It is also clearly shown that dissociation of CO* does not occur in the absence of H_2. Although it is envisaged that the adsorbed CO must be sequentially hydrogenated to methane, the steady-state concentrations of surface intermediates (e.g., formyl, CH_x*) in these steps are much lower compared with CO*, suggesting that they are rapidly and irreversibly converted and, consequently, present only at very low coverages.

With the present spectroscopic and kinetic data, it is, however, still difficult to identify the rate-controlling step during CO_2 methanation on Ru/Al_2O_3. Solymosi et al. ruled out the possibility of CO_2 dissociation (formation of adsorbed CO) being the rate-determining step based on the higher activation energy of CO methanation than that of CO_2 methanation on Ru/Al_2O_3 [17]. Bartholomew et al. concluded that the dissociation of CO* is the rate-determining step in CO_2 methanation over Ni/SiO_2 on the basis of kinetic modeling results using Langmuir–Hinshelwood expressions. As the evolution patterns of important surface species (bicarbonate, formate and adsorbed CO) on Ru/Al_2O_3 are similar to those on Pd/Al_2O_3 in our previous study, where the dissociation of CO* was proposed to be the rate-determining step, we argue that

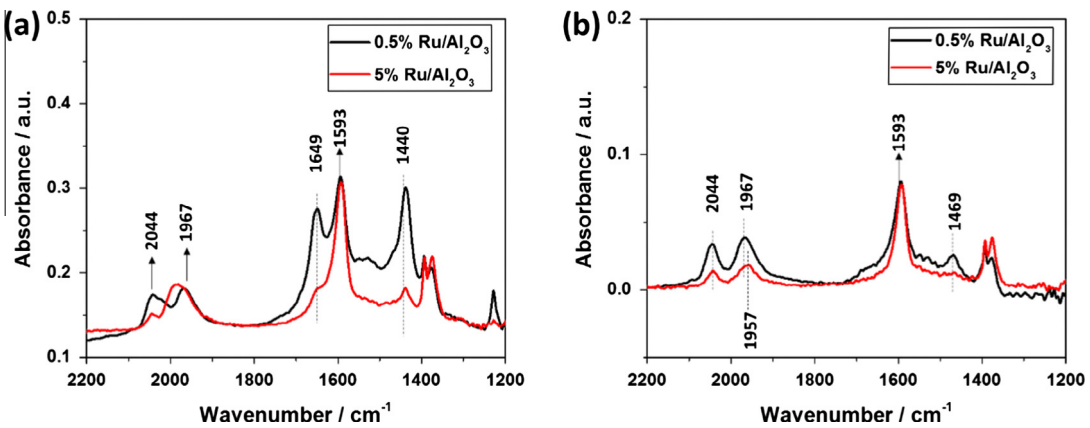

Fig. 5. DRIFT spectra collected at 503 K after 20 min in the feed gas of (a) $CO_2 + H_2$ and after 20 min in (b) H_2 switched from $CO_2 + H_2$ over 0.5% and 5% Ru/Al_2O_3.

the reaction between adsorbed H and adsorbed CO, rather than other steps, is the rate-determining step in CO_2 methanation also on Ru/Al_2O_3. Next, we present the results of our kinetic modeling study that support the proposed mechanistic sequence discussed above.

3.3. Kinetic modeling and assessments

The proposed sequence of elementary and lumped steps is listed in Tables 2 and 3. A H_2 molecule dissociates on the Ru surface into two chemisorbed H-atoms (Step 1). This step is known to be sufficiently fast on Group VIII transition metals to be considered quasi-equilibrated during the methanation reaction [55]. The other reactant, CO_2, is converted on the surface via a series of surface reactions (Steps 2–5), including the formation of bicarbonate (Step 2), H-assisted decomposition of bicarbonate to surface formate species (Step 3) followed by decomposition of the formate species into chemisorbed CO (Steps 4–5), as proposed by Renken et al. [26] and evidenced in our *in situ* transient DRIFTS–MS study. Note that the chemisorbed CO_2 in the form of bicarbonate and formate is mainly associated with the support surface, as suggested by Shelef [56] and Solymosi et al. [17]. In that sense, the quasi-equilibrated steps 2 and 3 in Tables 2 and 3 should be regarded as lumped steps including a migration step of bicarbonates (it is unstable according to our DRIFTS experiments and its migration should occur rapidly in order not to limit the methanation kinetics) from the support to the Ru surface. Only the formate formed at the metal-support interface is regarded as the reactive formate directly participating in the reaction (i.e., $HCOO^*$ in step 4). Due to the slow rate of conversion of formate at the interface, the formate migrates from the interface to the support under its gradient concentration, becoming irrelevant to the reaction. As it is conceptually difficult to imagine adsorbed CO to be formed within one elementary step between $HCOO^*$ and adsorbed H, we assumed the intermediacy of a formyl species, i.e., HCO^* (ads) which might be present only in very low surface coverage and thus could not be detected in the IR spectra. The surface reaction of chemisorbed CO and activated hydrogen atom may proceed in two pathways: (I) $CO^* + H^* = C^* + OH^*$ (Step I-6 in Table 2) and (II) $CO^* + H^* = CH^* + O^*$ (Step II-6 in Table 3). Methane is formed via further hydrogenation of carbon species like C^* and CH_x^* (Steps I-7 and 9–11) and desorption (Step 12), steps that are irrelevant to the overall methanation kinetics. Concomitantly, oxygen species (O^* and OH^*) are converted via H-addition reactions (Steps II-7 and 8) followed by water desorption (Step 13). Several elementary steps such as CO desorption in side reactions including CO formation were omitted from the proposed sequence owing to the fact that they are kinetically irrelevant for the methane formation and side reactions only occur to a small or even negligible extent over the Ru/Al_2O_3 catalysts under the conditions applied in this study. As discussed earlier, the surface sites (*) invoked in the proposed mechanistic sequence should count only those surface Ru atoms that are not irreversibly covered by strongly adsorbed CO species, rather than all the exposed surface Ru atoms. The fraction of these active Ru sites, however, is not precisely known at this stage. Therefore, the modeling results presented below were still based upon an inaccurate proxy (i.e., total surface atoms) for the "actual" TOFs. This would lead to uncertainties in the rate constant for the RDS (k_6), but there would be no effects on the regressed thermodynamic constants and activation enthalpies.

Table 2
Proposed sequence of elementary and lumped steps for CO_2 hydrogenation over Ru/Al_2O_3 catalysts (mechanism I).

Step	Reaction	Assumption	Constants
1	$H_2(g) + 2^* = 2H^*$	Quasi-equilibrium step	K_1
2	$CO_2 + OH^* = HCO_3^*$	Quasi-equilibrium step	K_2
3	$HCO_3^* + H^* = HCOO^* + OH^*$	Quasi-equilibrium step	K_3
4	$HCOO^* + H^* = HCO^* + OH^*$	Quasi-equilibrium step	K_4
5	$HCO^* + {}^* = CO^* + H^*$	Quasi-equilibrium step	K_5
I-6	$CO^* + H^* = C^* + OH^*$	Rate determining step	k_6
I-7	$C^* + H^* = CH^* + {}^*$	Low coverage of C^*	
8	$OH^* + H^* = H_2O^* + {}^*$	Irreversible	k_8
9	$CH^* + H^* = CH_2^* + {}^*$	Low coverage of CH^*	
10	$CH_2^* + H^* = CH_3^* + {}^*$	Low coverage of CH_2^*	
11	$CH_3^* + H^* = CH_4^* + {}^*$	Low coverage of CH_3^*	
12	$CH_4^* = CH_4(g) + {}^*$	Low coverage of CH_4^*	
13	$H_2O^* = H_2O(g) + {}^*$	Low coverage of H_2O^*	

Table 3
Proposed sequence of elementary and lumped steps for CO_2 hydrogenation over Ru/Al_2O_3 catalysts (mechanism II).

Step	Reaction	Assumption	Constants
1	$H_2(g) + 2^* = 2H^*$	Quasi-equilibrium step	K_1
2	$CO_2 + OH^* = HCO_3^*$	Quasi-equilibrium step	K_2
3	$HCO_3^* + H^* = HCOO^* + OH^*$	Quasi-equilibrium step	K_3
4	$HCOO^* + H^* = HCO^* + OH^*$	Quasi-equilibrium step	K_4
5	$HCO^* + {}^* = CO^* + H^*$	Quasi-equilibrium step	K_5
II-6	$CO^* + H^* = CH^* + O^*$	Rate determining step	k_6
II-7	$O^* + H^* = OH^*$	Low coverage of O^*	
8	$OH^* + H^* = H_2O^* + {}^*$	Irreversible	k_8
9	$CH^* + H^* = CH_2^* + {}^*$	Low coverage of CH^*	
10	$CH_2^* + H^* = CH_3^* + {}^*$	Low coverage of CH_2^*	
11	$CH_3^* + H^* = CH_4^* + {}^*$	Low coverage of CH_3^*	
12	$CH_4^* = CH_4(g) + {}^*$	Low coverage of CH_4^*	
13	$H_2O^* = H_2O(g) + {}^*$	Low coverage of H_2O^*	

3.3.1. Langmuir–Hinshelwood type models for mechanisms I and II

As shown in Table S1, a Langmuir–Hinshelwood type kinetics model for methane formation over Ru/Al_2O_3 catalyst via mechanism I in Table 2 is derived based on the sequence of steps and assumptions listed in Table 2. The hydrogenation of CO^* species was assumed to be the rate-determining step (Step 6) based on the discussion above. All prior steps (Steps 1-5) were assumed to be in quasi-equilibrium, while all successive steps, except for step 8, were assumed to be kinetically irrelevant as the coverage of the intermediates (C^*, CH_x^* and H_2O^*) was negligible and the corresponding rate constants were much larger than those of the rate-determining step, as suggested in the literature [57–59]. The rate equation is shown as Eq. (1), with the detailed derivations and assumptions shown in the Supporting Information:

$$r = \frac{\sqrt{k_6 k_8 K_2 K_3 K_4 K_5 P_{CO_2}}\,(K_1 P_{H_2})^{3/4}}{\left(1 + \sqrt{K_1 P_{H_2}} + \sqrt{K_1 P_{H_2}} K_2 K_3 P_{CO_2} + \sqrt{\sqrt{K_1 P_{H_2}} K_2 K_3 K_4 K_5 P_{CO_2}}\left(\sqrt{\frac{k_8}{k_6}} + \sqrt{\frac{k_8}{k_6}}\right)\right)^2} \quad (1)$$

Similarly, another Langmuir–Hinshelwood type kinetics model (Table S2) for methane formation over Ru/Al_2O_3 catalyst via mechanism II in Table 3 is derived based on the sequence of steps and assumptions listed in Table 3. The hydrogenation of CO^* species was assumed to be the rate-determining step (Step 6). All prior steps (Steps 1-5) were assumed to be in quasi-equilibrium while all successive steps except for step 8 were assumed to be kinetically irrelevant, as discussed for mechanism I. The kinetic expression for methane formation along mechanism II is in the same mathematical form as that derived for mechanism I (Eq. (1)), indicating that the two mechanisms are indistinguishable from kinetic measurements. Note, however, that the rate constant k_6 in Eq. (II-11) in Table S2 refers to the rate constant for $CO^* + H^* = CH^* + O^*$ while the rate constant k_6 in Eq. (I-11) in Table S2 refers to the rate constant for $CO^* + H^* = C^* + OH^*$. Most likely, the exact molecular-level details for the rate-determining step will only be accessible from theoretical evaluations which are beyond the scope of the present work.

3.3.2. Assessments of the regressed kinetic and thermodynamic constants and related energetics

TOFs for methane formation obtained at low CO_2 conversion levels (<5.5%) under different reaction conditions (reaction temperature = 513–573 K; $P_{H_2} = 10 - 70$ kPa; $P_{CO_2} = 10 - 70$ kPa) were fitted with the derived Langmuir–Hinshelwood type rate expression (Eq. (1)) to obtain equilibrium and rate constants listed in Tables 2 and 3. Parity plots for estimated and experimental TOFs for methane formation over Ru/Al_2O_3 catalysts are depicted in Fig. 6. All experimental TOF data align on the diagonal line with a slope of unity, indicating that both of the proposed mechanisms I and II are capable of explaining the measured kinetics for a wide range of conditions. The average relative errors for the fitting of TOF values for 0.5% Ru/Al_2O_3 and 5% Ru/Al_2O_3 are 3.1% and 2.9%, respectively. The equilibrium constants or their combinations (K_1, K_2K_3 and K_4K_5) and rate constants (k_6 and k_8) obtained from regression are listed in Table 4. The regressed equilibrium constants are very similar on 0.5% and 5% Ru/Al_2O_3 catalysts at the same reaction temperature, indicating that the Gibbs free energy changes of corresponding adsorption and surface transformation steps are nearly identical on the two catalysts. The coverages of different surface species can be estimated using these regressed thermodynamic constants. It turns out that the coverages of HCOO* (at interface sites) and OH* are much lower (combined for <3% of the total active sites) compared to those of CO* and H*, suggesting that CO* + H* is the most populated state for this reaction.

In addition, the regressed rate constants of CO* hydrogenation (k_6) on both catalysts are one order of magnitude smaller than the rate constants of OH* hydrogenation (k_8) at the same temperature, indicating CO* hydrogenation is indeed the rate determining step. Notably, the rate constant for the rate-determining step (k_6) is lower on the 0.5% Ru/Al_2O_3 catalyst than on 5% Ru/Al_2O_3 for each temperature, consistent with the experimental observation. However, as discussed in Section 3.2, the TOF values used in the kinetic modeling are the lower limits of the intrinsic TOF values due to the overestimation of active site population, and thus the rate constants calculated based on those TOF values also serve as the lower limits of the intrinsic rate constants for each elementary step.

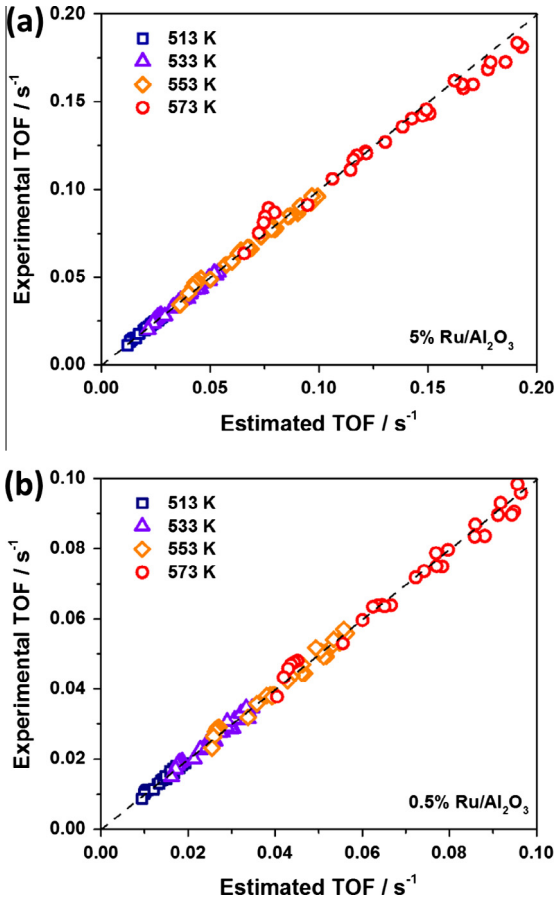

Fig. 6. Parity plot for estimated and experimental TOFs for methane formation over (a) 5% Ru/Al_2O_3 and (b) 0.5% Ru/Al_2O_3 catalysts at 513–573 K and different partial pressures of CO_2 and H_2 (10–70 kPa for both, total pressure 101 kPa balanced with He).

Table 4
The rate and equilibrium constants for CO_2 hydrogenation on 5% and 0.5% Ru/Al_2O_3 at 513–573 K and different partial pressures of CO_2 and H_2 (10–70 kPa for both, total pressure 101 kPa balanced with He).

Catalyst	T/K	Rate and equilibrium constants				
		K_1/kPa^{-1}	K_2K_3/kPa^{-1}	K_4K_5	k_6/s^{-1}	k_8/s^{-1}
5% Ru/Al_2O_3	**513**	0.010	0.00045	6.7	0.30	3.9
	533	0.005	0.00037	11.0	0.69	7.5
	553	0.003	0.00031	18.1	1.51	12.9
	573	0.002	0.00026	32.0	3.35	24.1
0.5% Ru/Al_2O_3	**513**	0.015	0.00044	6.3	0.17	3.4
	533	0.009	0.00035	10.2	0.36	5.9
	553	0.005	0.00030	17.6	0.68	10.8
	573	0.003	0.00027	27.2	1.40	17.2

Despite the overestimation of the rate constants, their temperature dependences and energetic parameters (enthalpies) derived from their temperature dependences are valid as intrinsic characteristics of elementary steps over each catalyst. Temperature dependences of the fitted equilibrium and rate constants are shown in Fig. S6. The energetic parameters (enthalpy and entropy changes) derived from Van't Hoff equation (enthalpy change for quasi-equilibrated steps), Arrhenius equation (activation enthalpy for the irreversible step) and Eyring–Polanyi equation (activation entropy for the irreversible step) are listed in Table 5 and depicted in Fig. 7. Both catalysts showed similar enthalpy changes for hydrogen adsorption (ΔH_1, −63.6 kJ/mol for 5% Ru/Al_2O_3 vs. −66.1 kJ/mol for 0.5% Ru/Al_2O_3), CO_2 chemisorption to form formate ($\Delta H_2 + \Delta H_3$, −22.3 kJ/mol for 5% Ru/Al_2O_3 vs. −19.8 kJ/mol for 0.5% Ru/Al_2O_3), and formate decomposition to form CO* ($\Delta H_4 + \Delta H_5$, 63.4 kJ/mol for 5% Ru/Al_2O_3 vs. 60.2 kJ/mol for 0.5% Ru/Al_2O_3). Note, in particular, that the enthalpy associated with hydrogen chemisorption (ΔH_1) is in good agreement with experimental value (−69 kJ/mol at $\theta_H = 0.2$ on Ru(0001)) reported by Ertl et al. [60]. The nearly identical enthalpies associated with those key quasi-equilibrated steps provide a similar energy for the combination of surface species (CO* + OH* + H*, −22.6 kJ/mol for 5% Ru/Al_2O_3 vs. −25.4 kJ/mol for 0.5% Ru/Al_2O_3 referenced to initial state with gas phase CO_2, H_2 and unoccupied Ru surface, Fig. 7) over both catalysts suggesting that the difference in the catalytic activity on these two catalysts (TOFs and apparent activation energy) does not originate from any enhancing or weakening in adsorption of key reaction intermediates.

Remarkably higher activation enthalpies were obtained on 5% Ru/Al_2O_3, on the basis of kinetic modeling results, for both CO* hydrogenation ($\Delta H_6^{\ddagger}$, 98.5 kJ/mol for 5% Ru/Al_2O_3 vs. 85.0 kJ/mol for 0.5% Ru/Al_2O_3) and OH* hydrogenation reactions ($\Delta H_8^{\ddagger}$, 73.8 kJ/mol for 5% Ru/Al_2O_3 vs. 67.3 kJ/mol for 0.5% Ru/Al_2O_3). The energy diagrams for both reactions (Fig. 7) suggest that such differences in activation enthalpy lie in the fact that the transition states for both steps are more stabilized on the 0.5% Ru/Al_2O_3 catalyst, probably due to a stronger binding of the transition state complex to under-coordinated sites (edge and corner), which are more abundant in catalysts with smaller Ru nanoparticles. However, the higher activation enthalpy over 5% Ru/Al_2O_3 must have been

Table 5
Energetic parameters for CO_2 hydrogenation on 5% and 0.5% Ru/Al_2O_3 at 513–573 K and different partial pressures of CO_2 and H_2 (10–70 kPa for both, total pressure 101 kPa balanced with He).

Catalyst	Enthalpy (kJ/mol) and entropy (J/mol/K)						
	ΔH_1	$\Delta H_2 + \Delta H_3$	$\Delta H_4 + \Delta H_5$	$\Delta H_6^{\ddagger}$	$\Delta H_8^{\ddagger}$	$\Delta S_6^{\ddagger}$ [a]	$\Delta S_8^{\ddagger}$ [a]
5% Ru/Al_2O_3	−63.6 ± 1.5	−22.3 ± 0.2	63.4 ± 3.0	98.5 ± 1.5	73.8 ± 2.2	−48.4 ± 2.9	−75.2 ± 4.3
0.5% Ru/Al_2O_3	−66.1 ± 2.4	−19.8 ± 1.9	60.2 ± 1.6	85.0 ± 2.0	67.3 ± 1.8	−79.3 ± 3.9	−89.0 ± 3.5

[a] Activation entropy calculated from TOFs obtained at 513 K using Eyring–Polanyi equation.

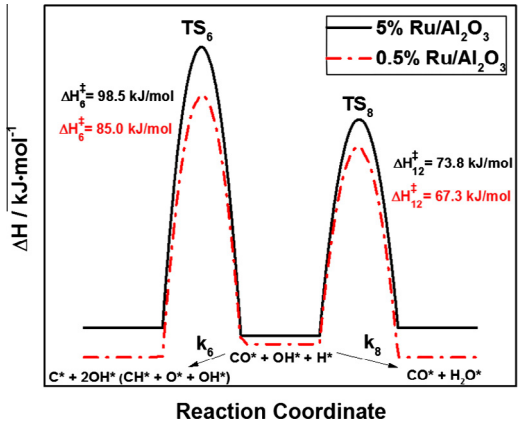

Fig. 7. Energy diagram of irreversible reaction steps during CO_2 methanation over (solid black line) 5% Ru/Al_2O_3 and (dotted red line) 0.5% Ru/Al_2O_3 catalysts. (The energies for $(C^* + 2OH^*)/(CH^* + O^* + OH^*)$ and $(CO^* + H_2O^*)$ are arbitrary and shown here only for illustration purposes.)

compensated by the more favorable entropic factors in order to account for the higher TOFs and intrinsic rate constants for the rate-determining step (k_6) on this catalyst, compared with 0.5% Ru/Al_2O_3 catalyst. The activation entropy change for both CO^* and OH^* hydrogenation steps over the two Ru/Al_2O_3 catalysts was calculated using data obtained at 513 K and listed in Table 5. Both steps (Steps I/II-6 and 8) feature negative activation entropies, suggesting a loss of degree of freedom toward the formation of transition states (i.e., "tight" transition states). In turn, we surmise that the transition states for Steps I/II-6 and 8 on 5% Ru/Al_2O_3 are not only less enthalpically stabilized but also less "tight" (i.e., $\Delta\Delta S_6^{\ddagger}$ ($\Delta S_6^{\ddagger}$ for 5% Ru/Al_2O_3 – $\Delta S_6^{\ddagger}$ for 0.5% Ru/Al_2O_3) = 30.9 J/mol/K and $\Delta\Delta S_8^{\ddagger}$ ($\Delta S_6^{\ddagger}$ for 5% Ru/Al_2O_3 – $\Delta S_6^{\ddagger}$ for 0.5% Ru/Al_2O_3) = 13.8 J/mol/K; Table 4), leading to smaller rate constants for both steps (Table 3). Note that these differences in activation entropies represent upper limits due to the fact that the difference in the "actual" TOFs (normalized to the number of active surface sites rather than all surface sites) between the two catalysts has been overestimated, as discussed in Section 3.2.

4. Conclusions

Steady-state kinetic and transient IR spectroscopic measurements suggest that the mechanism for and the surface species involved in CO_2 methanation do not change with the size of Ru particles in the studied range of Ru dispersions and reaction conditions. In the absence of adsorbed H, CO_2 does not dissociate directly to CO^* and O^* on Ru/Al_2O_3 catalysts; instead, it reacts with a hydroxyl on Al_2O_3 to form a bicarbonate, which, in turn, reacts with adsorbed hydrogen to yield a formate. Formates near the Ru particles (most likely at the metal/oxide interface) can rapidly react with adsorbed H to produce adsorbed CO, most likely via more than one elementary step. Remarkably, we find that only a portion of the CO^* is reactive toward adsorbed H on Ru, leading eventually to CH_4 formation. The other CO^* is inactive toward further methanation and present mainly in geminal di-carbonyl form adsorbed on low coordination Ru sites. These low-coordinated sites are more prevalent on the surface of smaller Ru particles than on larger Ru particles, resulting in the lower rates for CO_2 methanation on the former structure. Hereby, we envision that a tailored design and synthesis of Ru catalysts with large particles that minimize the possibility of gem-di-carbonyl formation could facilitate CO_2 methanation. The kinetic data are fully consistent with a Langmuir–Hinshelwood type mechanism involving all the spectroscopically detectable species and H-assisted dissociation of the reactive CO(ads) species as the rate-determining step. The detailed evaluation of the kinetic and thermodynamic constants within this mechanistic model has also allowed us to gain a better understanding on the origin of the Ru particle size effect and the energetics for elementary steps, which will serve as a basis for theoretical assessments on these catalysts in the future.

Acknowledgments

The catalyst preparation and catalytic measurements were supported by a Laboratory Directed Research and Development (LDRD) project. The authors gratefully acknowledge the financial support of this work by the US Department of Energy (DOE), Office of Science, Office of Basic Energy Sciences, Chemical Sciences, Geosciences, and Biosciences Division.

Appendix A. Supplementary material

Supplementary data associated with this article can be found, in the online version, at http://dx.doi.org/10.1016/j.jcat.2016.02.001.

References

[1] G.A. Somorjai, Catal. Rev. 23 (1981) 189–202.
[2] H. Arakawa, M. Aresta, J.N. Armor, M.A. Barteau, E.J. Beckman, A.T. Bell, J.E. Bercaw, C. Creutz, E. Dinjus, D.A. Dixon, K. Domen, D.L. DuBois, J. Eckert, E. Fujita, D.H. Gibson, W.A. Goddard, D.W. Goodman, J. Keller, G.J. Kubas, H.H. Kung, J.E. Lyons, L.E. Manzer, T.J. Marks, K. Morokuma, K.M. Nicholas, R. Periana, L. Que, J. Rostrup-Nielson, W.M.H. Sachtler, L.D. Schmidt, A. Sen, G.A. Somorjai, P.C. Stair, B.R. Stults, W. Tumas, Chem. Rev. 101 (2001) 953–996.
[3] M. Aresta, A. Dibenedetto, A. Angelini, Chem. Rev. 114 (2014) 1709–1742.
[4] W. Wang, S.P. Wang, X.B. Ma, J.L. Gong, Chem. Soc. Rev. 40 (2011) 3703–3727.
[5] T.v. Herwijne, H.V. Doesburg, W.A. Dejong, J. Catal. 28 (1973) 391–402.
[6] J.A. Dalmon, G.A. Martin, J. Chem. Soc., Faraday Trans. I 75 (1979) 1011–1015.
[7] T. Inui, M. Funabiki, M. Suehiro, T. Sezume, J. Chem. Soc., Faraday Trans. I 75 (1979) 787–802.
[8] J.L. Falconer, A.E. Zagli, J. Catal. 62 (1980) 280–285.
[9] G.D. Weatherbee, C.H. Bartholomew, J. Catal. 68 (1981) 67–76.
[10] G.D. Weatherbee, C.H. Bartholomew, J. Catal. 77 (1982) 460–472.
[11] F. Solymosi, A. Erdőhelyi, M. Lancz, J. Catal. 95 (1985) 567–577.
[12] F. Solymosi, A. Erdőhelyi, J. Mol, Catal. 8 (1980) 471–474.
[13] E. Ramaroson, R. Kieffer, A. Kiennemann, J. Chem. Soc., Chem. Commun. (1982) 645–646.
[14] J.H. Kwak, L. Kovarik, J. Szanyi, ACS Catal. 3 (2013) 2094–2100.
[15] X. Wang, H. Shi, J.H. Kwak, J. Szanyi, ACS Catal. (2015) 6337–6349.
[16] S. Eckle, M. Augustin, H.G. Anfang, R.J. Behm, Catal. Today 181 (2012) 40–51.
[17] F. Solymosi, A. Erdohelyi, M. Kocsis, J. Chem. Soc., Faraday Trans. I 77 (1981) 1003–1012.
[18] E. Zagli, J.L. Falconer, J. Catal. 69 (1981) 1–8.
[19] P.J. Lunde, F.L. Kester, J. Catal. 30 (1973) 423–429.
[20] J.H. Kwak, L. Kovarik, J. Szanyi, ACS Catal. 3 (2013) 2449–2455.

[21] Z. Kowalczyk, K. Stolecki, W. Rarog-Pilecka, E. Miskiewicz, E. Wilczkowska, Z. Karpiniski, Appl. Catal. A – Gen. 342 (2008) 35–39.
[22] J.M. Rynkowski, T. Paryjczak, A. Lewicki, M.I. Szynkowska, T.P. Maniecki, W.K. Jozwiak, React. Kinet. Catal. Lett. 71 (2000) 55–64.
[23] S.T. Zhang, H. Yan, M. Wei, D.G. Evans, X. Duan, RSC Adv. 4 (2014) 30241–30249.
[24] Y. Traa, J. Weitkamp, Chem. Eng. Technol. 22 (1999) 291–293.
[25] G.D. Weatherbee, C.H. Bartholomew, J. Catal. 87 (1984) 352–362.
[26] M. Marwood, R. Doepper, A. Renken, Appl. Catal. A – Gen. 151 (1997) 223–246.
[27] S. Scire, C. Crisafulli, R. Maggiore, S. Minico, S. Galvagno, Catal. Lett. 51 (1998) 41–45.
[28] M.R. Prairie, A. Renken, J.G. Highfield, K.R. Thampi, M. Gratzel, J. Catal. 129 (1991) 130–144.
[29] T. Iizuka, Y. Tanaka, K. Tanabe, J. Catal. 76 (1982) 1–8.
[30] F. Solymosi, A. Erdőhelyi, T. Bansagi, J. Chem. Soc., Faraday Trans. I. 77 (1981) 2645–2657.
[31] F. Solymosi, A. Erdőhelyi, T. Bánsági, J. Catal. 68 (1981) 371–382.
[32] F. Solymosi, A. Erdőhelyi, M. Kocsis, J. Catal. 65 (1980) 428–436.
[33] T. Inoue, T. Iizuka, K. Tanabe, Appl. Catal. 46 (1989) 1–9.
[34] T. Iizuka, Y. Tanaka, K. Tanabe, J. Mol. Catal. 17 (1982) 381–389.
[35] A. Erdőhelyi, M. Pásztor, F. Solymosi, J. Catal. 98 (1986) 166–177.
[36] M.A. Henderson, S.D. Worley, J. Phys. Chem. 89 (1985) 1417–1423.
[37] R.M. Koros, E.J. Nowak, Chem. Eng. Sci. 22 (1967) 470.
[38] J. Sirita, S. Phanichphant, F.C. Meunier, Anal. Chem. 79 (2007) 3912–3918.
[39] C. Morterra, A. Zecchina, S. Coluccia, A. Chiorino, J. Chem. Soc., Faraday Trans. I 73 (1977) 1544–1560.
[40] A. Vimont, J.C. Lavalley, A. Sahibed-Dine, C.O. Arean, M.R. Delgado, M. Daturi, J. Phys. Chem. B 109 (2005) 9656–9664.
[41] C. Morterra, G. Magnacca, Catal. Today 27 (1996) 497–532.
[42] A.M. Turek, I.E. Wachs, E. Decanio, J. Phys. Chem. 96 (1992) 5000–5007.
[43] J.B. Peri, J. Phys. Chem. 70 (1966) 3168–3179.
[44] C. Morterra, L. Orio, Mater. Chem. Phys. 24 (1990) 247–268.
[45] N.D. Parkyns, J. Phys. Chem. 75 (1971) 526.
[46] J. Szanyi, J.H. Kwak, Phys. Chem. Chem. Phys. 16 (2014) 15117–15125.
[47] J. Szanyi, J.H. Kwak, Phys. Chem. Chem. Phys. 16 (2014) 15126–15138.
[48] F. Solymosi, J. Raskó, J. Catal. 115 (1989) 107–119.
[49] A. Paredes-Nunez, D. Lorito, N. Guilhaume, C. Mirodatos, Y. Schuurman, F.C. Meunier, Catal. Today 242 (2015) 178–183.
[50] D. Lorito, A. Paredes-Nunez, C. Mirodatos, Y. Schuurman, F.C. Meunier, Catal. Today 259 (2016) 192–196.
[51] S. Eckle, Y. Denkwitz, R.J. Behm, J. Catal. 269 (2010) 255–268.
[52] E. Guglielminotti, A. Zecchina, A. Bossi, M. Camia, J. Catal. 74 (1982) 240–251.
[53] A. Zecchina, E. Guglielminotti, A. Bossi, M. Camia, J. Catal. 74 (1982) 225–239.
[54] S.Y. Chin, C.T. Williams, M.D. Amiridis, J. Phys. Chem. B 110 (2006) 871–882.
[55] A. Hellman, E.J. Baerends, M. Biczysko, T. Bligaard, C.H. Christensen, D.C. Clary, S. Dahl, R. van Harrevelt, K. Honkala, H. Jonsson, G.J. Kroes, M. Luppi, U. Manthe, J.K. Norskov, R.A. Olsen, J. Rossmeisl, E. Skulason, C.S. Tautermann, A.J. C. Varandas, J.K. Vincent, J. Phys. Chem. B 110 (2006) 17719–17735.
[56] R.A. Dallabetta, M. Shelef, J. Catal. 48 (1977) 111–119.
[57] M. Nawdali, H. Ahlafi, G.M. Pajonk, D. Bianchi, J. Mol. Catal. A – Chem. 162 (2000) 247–256.
[58] S.Y. Wang, S.H. Moon, M.A. Vannice, J. Catal. 71 (1981) 167–174.
[59] S. Vanho, P. Harriott, J. Catal. 64 (1980) 272–283.
[60] H. Shimizu, K. Christmann, G. Ertl, J. Catal. 61 (1980) 412–429.